Journal of Non-Crystalline Solids 450 (2016) 18–22

Contents lists available at ScienceDirect

Journal of Non-Crystalline Solids

journal homepage: www.elsevier.com/locate/jnoncrysol

Rare earth-dependent trend of the glass transition activation energy of doped phosphate glasses: Calorimetric analysis

Mariana Sendova [a,*], José A. Jiménez [b,1], Chandler Honaman [a]

[a] Optical Spectroscopy & Nano-Materials Lab, New College of Florida, Sarasota, FL 34243, USA
[b] Department of Chemistry, University of North Florida, Jacksonville, FL 32224, USA

ARTICLE INFO

Article history:
Received 22 March 2016
Received in revised form 23 May 2016
Accepted 26 July 2016
Available online 1 August 2016

Keywords:
Calorimetry
Activation energy
Glass transition
Phosphate glasses

ABSTRACT

Eight types of rare earth (RE)-doped barium phosphate glasses have been studied by differential scanning calorimetry (DSC) in the glass transition region. Proposed is a concurrent analysis of a family of heat flow data assessing the glass transition activation energies. Furthermore, the DSC data indicate correlation of the activation energy with the ionic radius of the RE dopant, in agreement with the bond strength modifications suggested by the Raman data. Estimated activation energy values between 4.0(2) eV and 4.9(2) eV are in support of P—O bond exchange theory of the glass transition. It is proposed that the measured activation energy can serve as a relative quantifier of the intermediate-range order of the glass structure.

1. Introduction

Rare earth (RE) ions, also referred to as lanthanides, are the active constituents of many optical materials. Much of today's cutting-edge optical technology and emerging innovations are enabled by the RE's unique properties and interdependence with the embedding glass matrix [1,2]. In recent years, there has been steadily an increasing number of studies on the relationships between the RE and host electronic states and how they affect the optical properties of specific interest for telecommunication and solar energy conversion. However, RE-dependent trends of the intermediate-range order of the host glass matrix, and stemming from them activation energy of glass transition has not been elucidated yet. Furthermore, it appears that the activation energy for any kinetic process in an amorphous glassy matrix can serve as a reliable, relative quantifier of the intermediate-range order of the underlining structure [3]. When the glass is heated across the glass transition region, a time-dependent response of its physical properties (e.g., volume, enthalpy, viscosity) occurs [4,5]. The unrelaxed, glassy state approaches equilibrium, over a finite period of time. This gradual approach of the physical properties to their equilibrium values is due to structural relaxation, i.e., equilibration. Therefore, the glass transition temperature, T_g, is not a constant specific to the chemical composition of the glass. The glass transition is a kinetic transition [6] depending on multiple parameters, such as heating and cooling rates, and the thermal history of the material [7].

In this work, we aim to establish the conditions under which the apparent activation energy of the glass transition of RE-doped barium phosphate glasses can be assessed with differential scanning calorimetry (DSC), concomitant with Raman spectroscopy. Furthermore, the study attempts to answer the question of how the RE ionic radius impacts the activation energy.

2. Experimental

The glasses were made with a $50P_2O_5$:50BaO (mol%) composition, matrix which has been previously proposed by Uchida et al. [8] for nonlinear optical studies of metallic nanoparticles given its intrinsic high metal solubility. These were prepared from high purity compounds (P_2O_5 and $BaCO_3$) by the melt-quenching technique [9]. In this procedure, batch materials are melted in porcelain crucibles at 1150 °C for 15 min under normal atmospheric conditions and immediately quenched. RE element doping was done by adding their corresponding oxides quantities in mol%, relative to the network former P_2O_5. Eight types of glass samples were prepared for the present study. They are referred to as (doping oxide): Pr glass (2% Pr_2O_3); Nd glass (2% Nd_2O_3); Sm glass (2% Sm_2O_3); Gd glass (2% Gd_2O_3); Dy glass (2% Dy_2O_3); Ho glass (2% Ho_2O_3); Er glass (2% Er_2O_3); and Yb glass (2% Yb_2O_3).

The heat flow data were acquired with a TA Instruments Q20 differential scanning calorimeter. In this set-up there is one heating element and a cell with two identical pedestals - one for a sample pan and the other for a reference pan. Aluminum pans were used for the sample and the empty reference one. The studied samples were ~75 mg. During

* Corresponding author.
E-mail address: sendova@ncf.edu (M. Sendova).
[1] Present address: Functional Films Lab, BASF Corporation, 2655 Route 22 West, Union, NJ 07083, USA.

http://dx.doi.org/10.1016/j.jnoncrysol.2016.07.035
0022-3093/

the measurements, the rate of temperature increase of the heating element was kept constant. The different heat capacity of the sample and its reference induces a temperature difference, which is used by the DSC software to calculate the heat flow. Further on, the heat flow, Φ, in mW, was analyzed as a function of temperature. The glasses were heated from the non-equilibrium glassy state to the equilibrium state, across the T_g region. For each sample, data were collected in the temperature range 460–590 °C for four heating rates, q: 8 °C/min; 25 °C/min; 50 °C/min and 100 °C/min. For the Pr glass data were collected between 400 and 590 °C. The set of four constant heating rate heat flow curves, $\Phi_q(T)$ were analyzed. The cooling rates after each heating cycle was kept constant at ~86(2) °C/min. Two independent measurements were performed for each sample. The two independent set of data were used to estimate the sample related uncertainty. A baseline calibration was obtained by a temperature scan over the entire range with no pans in the DSC cell. The melting point of indium was used for temperature calibration. All measurements were performed following identical procedure, Fig. 1a. The samples were annealed in situ at 500 °C (450 °C for the Pr glass) for 40 min. The annealing around T_g of the glass samples was carried out to remove internal stress, thus minimizing sample to sample variations due to non-uniformity of the stress distribution.

Raman spectra were acquired using a Leica (Kaiser Optical Systems Inc.) DMLP microscope coupled to a Raman system from Kaiser Optical Systems Inc. (Ann Arbor, MI) The RamanRxn1TM analyzer (Kaiser Optical Systems Inc.) incorporates the thermoelectrically cooled charge coupled device detector for maximum sensitivity, InvictusTM (Kaiser Optical Systems Inc.) near-IR semiconductor laser with wavelength of 532 nm and holographic grating to provide fast, simultaneous full spectral collection of Raman data. The spectral resolution of the Raman system is about 5 cm^{-1}. The measurements were carried out at room temperature (RT) and at the annealing temperature.

3. Results and discussion

Four constant cooling rate cycles were performed to ensure the heating cycle onset is from the same metastable glass structure. Then, the family of four heat flow data sets, each obtained at constant heating rate, $\Phi_q(T)$ were analyzed. Fig. 1a illustrates the thermal histories for all samples and Fig. 1b summarizes the normalized heat flow data specifically for the Er glass. The rapid return to equilibrium above T_g appears as an "overshoot". Further on, four T_g values are determined from the heat flow data at the point of maximum slope in the transition region. The grey trace in Fig. 2 corresponds to the first derivative (right axis) of the heat flow trace (black, left axis) presented in the same graph. The overshoot temperature, T^+ is indicated as well. T^+ is determined from the point at which the first derivative is closest to zero (grey trace, Fig. 2).

The average T_g values of each type of glass at the corresponding heating rate, are summarized in Table 1. The uncertainty derived from

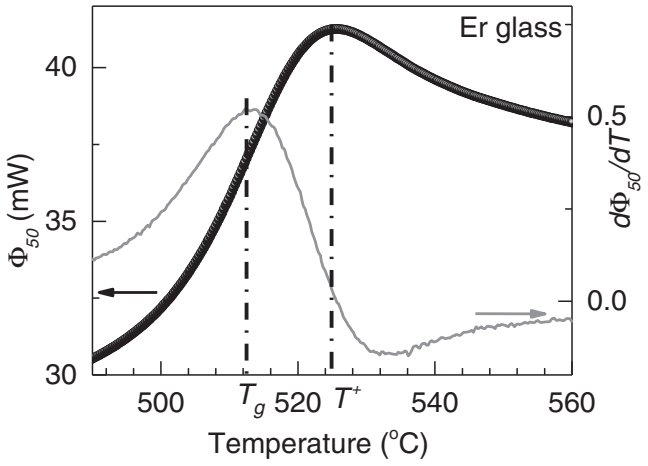

Fig. 2. Example for T_g assessment at the point of maximum slope of the heat flow curve $\Phi_{50}(T)$ for Er glass. The grey trace is the first derivative of the heat flow. The heating rate of 50 °C/min is indicated by the subscript.

measuring multiple samples is given in parenthesis. T_g is increasing with the heating rate in agreement with the delayed structural relaxation in the material [4]. Further on, the four average T_g values for each glass type are plotted in an Arrhenius-like plot suggested by Moynihan et al. for structural relaxation [10], Fig. 3:

$$\ln(q) \propto \frac{\Delta h^*}{RT_g} \tag{1}$$

where Δh^* is the activation energy for the glass transition and R is the universal gas constant.

While the T_g increases with the heating rate, the time interval in which the glass transition takes place is decreasing. The time scale of the process is a direct consequence of a structural relaxation driving the equilibration of the enthalpy. The authors propose the relaxation time, τ [s] to be estimated from the T^+ (vide supra) and T_g difference and the heating rate:

$$\tau = 2 \cdot \frac{(T^+ - T_g)}{q} \tag{2}$$

where q is in °C/s. Relaxation times from 20 s to 250 s are assessed for the RE glass series over the various heating rates in agreement of the range of enthalpic and viscosity relaxation times for alkali silicates reported by other authors [5,10]. For the Er glass, the estimated relaxation time values (open circles, Fig. 3 right axis) are 35 s (q = 50 °C/min); 53 s (25 °C/min); and 162 s (8 °C/min). The broad overshoot feature of the heat flow curve (I) in Fig. 1 (b) does not allow for estimation of the relaxation time with satisfactory accuracy and the authors deemed

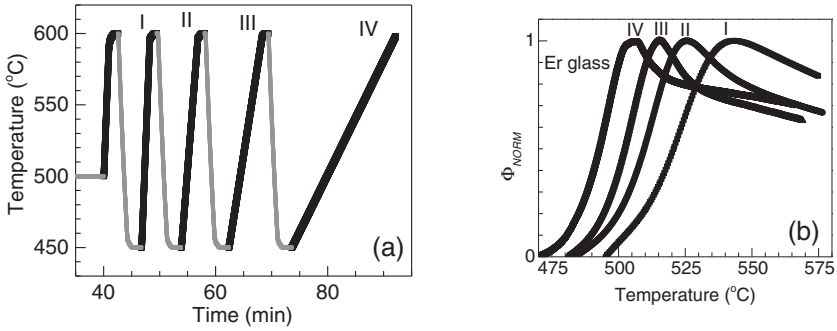

Fig. 1. (a) Thermal cycling procedure for all samples. Only the Pr glass was annealed at 450 °C. Data for the following heating segments were analyzed: I. q = 100 °C/min; II. q = 50 °C/min; III. q = 25 °C/min; IV. q = 8 °C/min. (b) Normalized heat flow data (Φ_{NORM}) for the Er glass corresponding to the thermal cycling procedure in (a).

Table 1
T_g, in °C, and the glass transition activation energy, for the eight RE-doped glasses.

Heating rate (°C/min)	Pr	Nd	Sm	Gd	Dy	Ho	Er	Yb
100	487 (3)	529 (3)	533 (2)	530 (1)	525 (1)	529 (4)	523.9 (6)	532 (1)
50	474 (1)	518 (2)	519.8 (9)	519.0 (6)	514.2 (1)	517 (2)	512.8 (7)	521.4 (9)
25	466 (1)	510 (1)	510.7 (5)	511.5 (3)	506.0 (1)	509.4 (6)	505.5 (6)	513.8 (2)
8	457.4 (4)	501.5 (1)	499.9	502.3 (2)	496.2 (2)	499.9 (2)	495.6 (3)	504.7 (1)
Activation energies								
Δh^* (eV)	4.0 (2)	4.2	4.4 (2)	4.7 (2)	4.5 (2)	4.5 (5)	4.7	4.9 (2)

appropriate to omit this point from the Arrhenius-like plot, Fig. 3 (open circles). As can be expected, the structural relaxation time decreases with temperature, following the Narayanaswamy's model [11].

$$\ln(\tau) \propto \frac{\Delta h_r^*}{RT_g} \tag{3}$$

where Δh_r^* is the structural relaxation activation energy.

Both Arrhenius-like plots for Er glass, Fig. 3, have the same slopes (54 kK^{-1}). The coefficient of correlation (R^2) is 0.96. Therefore, the data suggests that the assessed relaxation times represent the enthalpy equilibration time scales thus yielding the same activation energy $\Delta h_r^* = \Delta h^*$. The obtained $\Delta h^*/R$ values are in the range 47 to 57 kK and agree with the reported values for other glassy materials: B_2O_3 glass - 46 kK [10], 23 mol% K_2O - 77 mol% SiO_2 glass - 50.5 kK [10], G-11 glass 64.5 kK [4]. The average activation energy Δh^* in eV (last row in Table 1) is converted from the reduced glass transition activation energy $\Delta h^*/R$ in kK.

Fig. 4 summarizes the estimated glass transition activation energies as a function of the ionic radius [12] of the RE dopant modifier. It was assumed that the average rare earth coordination number is six (CN = 6) [13]. The largest activation energy of 4.9(2) eV is estimated for the Yb glass, while the lowest one - for Pr glass, 4.0(2) eV. Overall, 18% reduction of the activation energy is estimated in the studied RE glass series. The data are fitted with a straight line with a slope ~ 0.5 eV/0.1 Å. The correlation suggests that the lanthanide ionic size is affecting the overall "rigidity" of the glass network. Estimated six fold relaxation time decrease between the Yb glass (166 s at 504 °C) and Pr glass (28 s at 508 °C) provide further strong support for a declining "rigidity" of the glass network with the ionic size.

The basic building blocks of the phosphate glasses are the P-tetrahedra products of the formation of sp^3 hybrid orbitals by the phosphorus outer electrons ($3s^2 3p^3$). The fifth valence electron is promoted to a 3d orbital where strong π-bonding molecular orbitals are formed with oxygen 2p electrons [14,15]. The P-tetrahedra link through covalent bridging oxygens to form polymeric phosphate anions varying in length. The tetrahedra are classified using the Q^i terminology [16], where the superscript represents the number of bridging oxygens per tetrahedron. The modifier cations provide ionic bonds with the polymeric anions, holding the matrix together while preventing it from crystallization [17]. Neutron diffraction and Raman spectroscopy studies for mixed alkali phosphate glasses established that while the short-range order of the phosphorous-oxygen network is almost independent of the glass composition, the cation modifier environments depend on the cation size [18]. More specifically, in the same study Swenson et al. [18], after evaluating the Rb—O and Li—O bond lengths, reported that larger cations lead to a weaker modifier effect (longer bonds) in addition to an increased CN. The latter was successfully tested on the RE phosphate glass series with the Raman spectroscopy study presented below.

Nuclear magnetic resonance studies on various alkali silicate glasses [19,20] indicate that the glass transition involves Si—O bond breaking. Rates of exchange of silicon atoms among neighboring silicate tetrahedra implicating Si—O bond breaking have been measured and are shown to be closely related in time scale to viscosity relaxation and the time scale of the glass transition. Considering that the phosphate glasses have analogous tetrahedral short range structure as silicates, we propose that both glass systems share similar atomic glass transition mechanisms. Namely, the phosphate glass transition involves P—O bond breaking and reformation as expected for a phosphorus exchange (P—O bond exchange) between adjacent tetrahedral units. Furthermore, it was noted that the estimated glass transition activation energies, see Table 1, are comparable with the average P—O bond dissociation energies of ~4.8 eV in P_2O_5 glasses [21]. Therefore, the data suggest that the slowest structural relaxation rate is the rate of P—O bond exchange. Furthermore, this structural relaxation rate is responsible for the enthalpy relaxation in the glass transition range reported in this study.

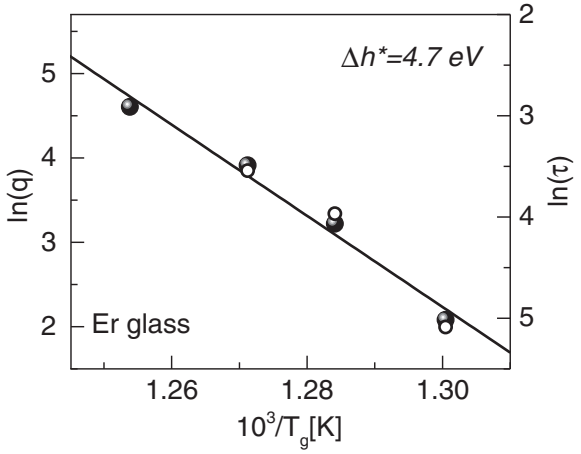

Fig. 3. Arrhenius-like plot for Er glass: q (left axis, solid symbols) is the heating rate in °C/min; τ (right axis, open symbols) is the relaxation time in seconds.

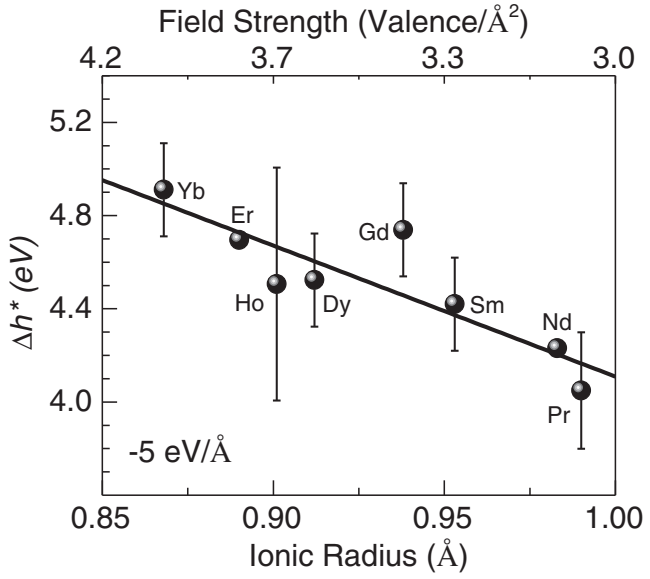

Fig. 4. Glass transition activation energy vs. the RE ionic radius [12] (bottom scale) and the field strength (top scale).

Table 2
Summary of Raman spectroscopy parameters associated to main bands in Fig. 5.

Glass	Temperature	ν_s(POP) (cm^{-1})	$\overline{\nu}_s$ (POP) (cm^{-1})	$\nu_s(PO_2)$ (cm^{-1})	$\overline{\nu}_s$ (PO_2) (cm^{-1})	I{ν(NBO)} / I{ν(BO)}
Yb	RT	687	705	1159	1130	2.1
glass	500 °C	681	698	1151	1124	
Pr	RT	689	707	1156	1118	2.5
glass	500 °C	684	699	1147	1113	

Raman spectroscopy has long been used to investigate the short-range structures of phosphate glasses. In this study we propose that Raman spectroscopy can be indicative of the intermediate-range structure as well. Fig. 4 shows normalized Raman spectra as obtained with excitation wavelength of 532 nm for the Yb and Pr glass as the most contrasting cases. The main Raman features for the studied glasses are detected in the range 600–1400 cm^{-1}. Table 2 summarizes the band positions and assignments of the two most intense bands. We propose that according to the phonon mode assignments [15,22,23,24], the entire range can be divided in two sections, see top axis in Fig. 5: (i) below 850 cm^{-1} – the range of the bridging oxygens (BO) in-chain symmetric stretching modes, ν_s(POP); and (ii) above 850 cm^{-1} – the range related mainly to the non-BO (NBO).

The NBO are the oxygens coordinating the RE cations. The Raman active NBO modes are those of the terminal tetrahedral groups Q^1 $\nu(PO_3)$, including the ones from dimers $\nu(P_2O_7)$ (970–1150 cm^{-1}) [24], and the NBO of the Q^2 and their out-of-chain symmetrical $\nu_s(PO_2)$ and asymmetrical $\nu_{as}(PO_2)$ stretching modes (1150–1400 cm^{-1}). The position of the $\nu_s(PO_2)$ and $\nu_{as}(PO_2)$ bands related to the symmetric and asymmetric stretching modes in connection to the NBO have been found to be cation dependent [22]. The dependency is through the size, charge, and the electronegativity of the modifying cations. Raman spectra in Fig. 5 shows that the symmetric stretching $\nu_s(PO_2)$ band position of the Yb glass slightly shifted, 3 cm^{-1}, toward higher wavenumber as compared to the Pr glass. The detected 'upshift' is an indication of stronger Q^2 NBO bonds in agreement with the established higher glass transition activation energy in Yb glass and the understanding that the glass transition is a result of increased frequency of P—O bond exchange. In addition, the relatively less intense $\nu(PO_3)$ (terminal Q^1 species) band in Yb glass is indicative of longer polymeric chains, in agreement with the higher activation energy of the Yb glass. The broad asymmetric feature between 630 and 830 cm^{-1} is an envelope of continuous distribution of ν_s(POP) frequencies inversely proportional to the phosphate chain length. Longer chains yield lower frequency components of the band and vice versa. The slight shift to lower energies of the ν_s(POP) band concurs with the possible presence of longer tetrahedral chains in the Yb glass. Further on, the two main Raman features are envelopes of multiple phonon modes reflecting two important structural statistical parameter distributions: chain length and NBO bond strength. Therefore, in addition to the main band position we propose statistical method for Raman glass network characterization. Deconvolution was deemed ineffective, since it is associated with considerable number of uncertain parameters. Therefore, instead of multi-peak fitting procedure, the BO and NBO ranges are integrated separately. In Table 2 the main band position and the mean Raman shift for the two terminal members in the RE doped glass series are compared. The integral intensity ratio I{ν(NBO)} / I{ν(BO)} at room temperature, Fig. 5a, is listed for comparison too. It is proposed that the relative integral intensity of the Raman bands in the NBO and BO range, I{ν(NBO)} / I{ν(BO)}, can serve as a spectroscopic estimate of the relative amount of NBO in the glasses at RT. Pr glass appears to have ~20% more NBO relative to the Yb glass, in agreement with the Pr glass which has ~23% lower apparent glass transition activation energy Table 1. Having in mind that the coordination of the RE cations is provided by the NBO, our Raman spectroscopy study is in agreement with Swenson et al. [18]. who reported neutron scattering data suggesting increased CN for larger cation modifiers. Furthermore, the larger CN is associated [18] with relative weakening of the modifier cation oxygen bond. Therefore, the larger RE ion size weakens the coordinating bonds, in agreement with the weaker ionic field strength, top axis in Fig. 4. The ionic field strength is estimated according to the Coulomb's law for electrostatic field strength of the RE ions. The ion size trend for activation energy reduction, presented in Fig. 4, supports a P—O bond exchange glass transition mechanism with the prevalent role played by the weakly attached NBO coordinating the RE cations. The latter affects the intermediate range glass structure, while the short range structure remains unaltered as suggested previously [18].

A Raman spectra comparison at RT and above the glass transition, 500 °C, is shown in Fig. 5b for the Pr glass. A lower wavenumber shift, ~5 cm^{-1}, of the ν_s(POP) band position P—BO bonds of the Q^2 species at 500 °C is in agreement with the thermally-induced bond weakening, Table 2. A lower wavenumber shift, ~8 cm^{-1}, of the $\nu_s(PO_2)$ band position, supports the overall thermal weakening of the P—NBO bonds of the Q^2 species, in agreement with the decreased intensity of the asymmetric mode $\nu_{as}(PO_2)$. Furthermore, thermally-induced weakening of the P—O bonds lead to increased probability of P—O bond exchange, and decreasing the structural relaxation times with temperature as estimated with the DSC measurements (vide supra).

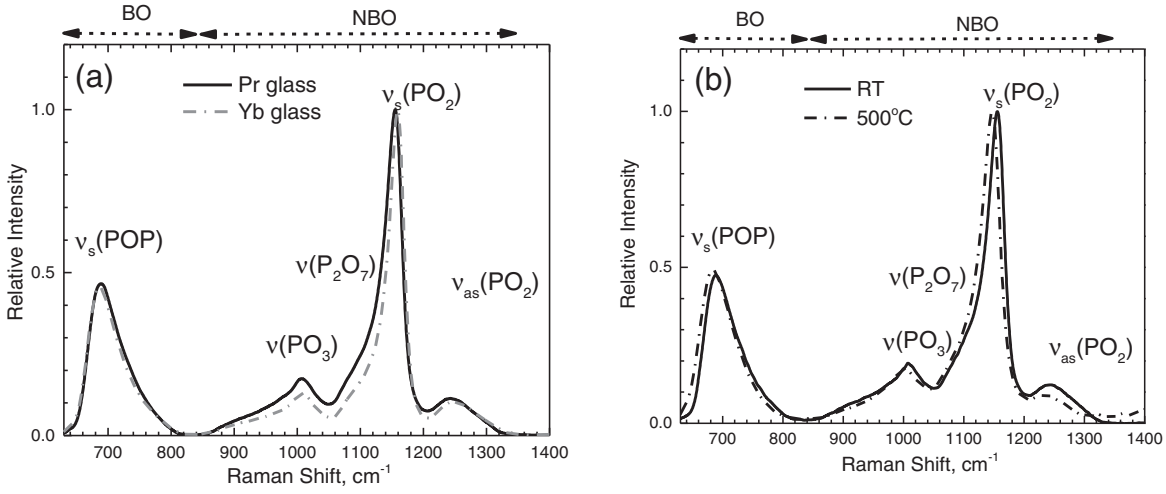

Fig. 5. Normalized Raman spectra and mode assignments for (a) the two extreme compositions, Yb and Pr glass and (b) Pr glass at room temperature (RT) and at 500 °C.

4. Conclusions

A concurrent analysis of a family of heat flow data has been realized in order to evaluate the glass transition activation energy of RE-doped phosphate glasses. The obtained values between 4.0(2) eV and 4.9(2) eV and the Raman spectroscopy analysis are in support of P—O bond exchange at the origin of the glass transition. Most importantly, a correlation between the activation energy and the ionic radius of the lanthanide dopant was indicated in agreement with the estimated relaxation times and the Raman spectroscopy Q species study. It is therefore proposed that the measured activation energy can serve as a relative quantifier of the intermediate range order of the glass structure.

Acknowledgements

M.S. is grateful for the private grant support of Tina and George Skestos.

References

[1] J.-C.G. Bünzli, S.V. Eliseeva, Lanthanide NIR luminescence for telecommunications, bioanalyses and solar energy conversion, J. Rare Earths 28 (2010) 824–842.
[2] C.W. Thiel, Y. Sun, R.L. Cone, Progress in relating rare-earth ion 4f and 5d energy levels to host bands in optical materials for hole burning, quantum information and phosphors, J. Mod. Opt. 49 (2002) 2399–2411.
[3] M. Sendova, J.A. Jiménez, R. Smith, N. Rudawski, Kinetics of copper nanoparticle precipitation in phosphate glass: an isothermal plasmonic approach, Phys. Chem. Chem. Phys. 17 (2015) 1241–1246.
[4] G.W. Scherer, Relaxation in Glass and Composites, Wiley, New York, 1986.
[5] S. Webb, Silicate melts: relaxation, rheology, and glass transition reviews of geophysics, Rev. Geophys. 35 (1997) 191–218.
[6] A.A. Chernov, Kinetic phase transitions, JETP 26 (1968) 1182–1186.
[7] R.D. Corsaro, Volume relaxation of dry and wet boron trioxide in the glass transformation range following a sudden change of pressure, Phys. Chem. Glasses 17 (1976) 13–22.
[8] K. Uchida, S. Kaneko, S. Omi, C. Hata, H. Tanji, Y. Asahara, A.J. Ikushima, T. Tokisaki, A. Nakamura, Optical nonlinearities of a high concentration of small metal particles dispersed in glass: copper and silver particles, J. Opt. Soc. Am. B 11 (1994) 1236–1273.
[9] J.A. Jiménez, J. Mater. Sci. 49 (2014) 4387–4393.
[10] C.T. Moynihan, A.J. Easteal, M.A. DeBolt, J. Tucker, Dependence of the fictive temperature of glass on cooling rate, J. Am. Ceram. Soc. 59 (1976) 12–16.
[11] O.S. Narayanaswamy, A model of structural relaxation in glass, J. Am. Ceram. Soc. 54 (1971) 491–497.
[12] R.D. Shannon, Revised effective ionic radii and systematic studies of interatomic distances in halides and chaleogenides, Acta Cryst A32 (1976) 751–767.
[13] R. Anderson, T. Brennan, G. Mountjoy, R.J. Newport, G.A. Saunders, An EXAFS study of rare-earth phosphate glasses in the vicinity of the metaphosphate composition, J. Non-Cryst. Solids 232–234 (1998) 286–292.
[14] D.W.J. Cruickshank, The role of 3d-orbitals in v-bonds between (a) silicon, phosphorus, sulphur, or chlorine and (b) oxygen or nitrogen, J. Chem. Soc. (1961) 5486–5504;
K.A.R. Mitchell, The use of outer d orbitals in bonding, Chem. Rev. 69 (1969) 157–178.
[15] R.K. Brow, Review: the structure of simple phosphate glasses, J. Non-Cryst. Solids 263–264 (2000) 1–28.
[16] F. Liebau, in: M. O'Keefe, A. Novrotsky (Eds.), Structure and Bonding in Crystals II, Academic Press, New York 1981, p. 197.
[17] J.E. Stanworth, Physical Properties of Glass, Clarendon Press, Oxford, 1950.
[18] J. Swenson, A. Matic, A. Brodin, L. Börjesson, W.S. Howells, Structure of mixed alkali phosphate glasses by neutron diffraction and Raman spectroscopy, Phys. Rev. B 58 (1998) 11331–11337.
[19] I. Farnan, J.F. Stebbins, The nature of the glass transition in a silica-rich oxide melt, Science 265 (1994) 1206–1209.
[20] L. S-B, J.K. Stebbins, E. Schneider, A. Pines, Diffusive motion in alkali silicate melts: an NMR study at high temperature, Geochim. Cosmochim. Acta 52 (1988) 527–538.
[21] V. Dimitrov, T. Komatsu, Polarizability, basicity, and chemical bonding of single and multicomponent oxide glasses, J. Chem. Technol. Metall. 50 (2015) 387–396.
[22] B.N. Nelson, G.J. Exarhos, Vibrational spectroscopy of cation–site interactions in phosphate glasses, J. Chem. Phys. 71 (1979) 2739–2747.
[23] D. Ilieva, D. Kovacheva, C. Petkov, G. Bogachev, Vibrational spectra of $R(PO_3)_3$ metaphosphates (R = Ga, In, Y, Sm, Gd, Dy), J. Raman Spectrosc. 32 (2001) 893–899.
[24] G. Le Saoût, P. Simon, F. Fayon, A. Blin, Y. Vaills, Raman and infrared study of $(PbO)_x(P_2O_5)_{(1-x)}$ glasses, J. Raman Spectrosc. 33 (2002) 740–746.